JOURNAL OF THEORETICAL AND APPLIED MECHANICS
60, 3, pp. 495-508, Warsaw 2022
https://doi.org/10.15632/jtam-pl/151819

THE INFLUENCE OF LOADING RATE ON THE MECHANICAL BEHAVIOR AND ENERGY EVOLUTION CHARACTERISTICS OF HARD AND SOFT ROCK UNDER TRIAXIAL COMPRESSION

Jihui Deng

China Coal Technology and Engineering Chongqing Design and Research Institute (Group) Co., Ltd., Chongqing, China

Chao Chen

China Coal Technology and Engineering Chongqing Design and Research Institute (Group) Co., Ltd., Chongqing, China; School of Civil Engineering, Chongqing University, Chongqing, China

Corresponding author Chao Chen, e-mail: 657616428@qq.com

Xiaoning Wu

China Coal Technology and Engineering Chongqing Design and Research Institute (Group) Co., Ltd., Chongqing, China

To investigate the influence of loading rate and confining pressure on the mechanical behavior and energy evolution characteristics of hard and soft rock, high strength sandstone and low strength granite were subjected to triaxial compression tests with different loading rates. The results show that significant differences exist in the stress-strain curves for sandstone and granite. The confining pressure has a significant effect on the stress-strain curve, while the loading rate has a smaller effect on the stress-strain curve. As the confining pressure increases, the peak axial strain, peak axial stress, total energy, elastic energy and dissipated energy of sandstone and granite increase, the proportion of dissipated energy to total energy of sandstone and the proportion of elastic energy to total energy of granite are reduced. As the loading rate goes up, the peak axial stress, total energy and elastic energy increase in both sandstone and granite. The ultimate failure pattern of sandstone is a typical single inclined plane shear failure, while the ultimate failure pattern of granite consists of a single inclined plane shear failure and a vertical split failure. The loading rate has no significant effect on the macroscopic failure pattern, the elastic and dissipated energies are proportional to the total energy of sandstone and granite.

Keywords: hard and soft rock, triaxial compression test, strength, deformation, failure pattern, energy evolution

1. Introduction

In the construction of many soft-hard interbedded rock masses, hard and soft rock often face the same confining pressure and excavation speed (Fig. 1). The confining pressure and excavation speed are two key factors affecting safety and progress of the rock engineering construction (Alam *et al.*, 2015; Fereidooni *et al.*, 2016; Kavvadas *et al.*, 2020). Furthermore, the mineral composition, grain size, shape and structure of hard and soft rock often have great differences. This leads to obvious differences in physical properties and mechanical behavior between hard rock and soft rock. The effects of confining pressure and loading rate on the mechanical behavior and energy evolution of hard and soft rock are also significantly different. Hence, it is of great significance to further explore the mechanical behavior and energy evolution of hard and soft rock under different confining pressure and loading rates.

The studies on the mechanical behavior and energy evolution of single hard and soft rocks have been extensively reported (Asem, 2019; Sengani, 2020; Pinazzi *et al.*, 2021). Chen *et al.* (2021) studied the effect of stress paths on the failure mechanism and progressive damage of hard-brittle rock, their results shown that an increase in the confining pressure was beneficial to improve the mechanical parameters of rock, but it reduced the brittle failure features. Karami and Tolooiyan (2020) investigated elastoplasticity of Australian soft rock based on a triaxial compression test. They found that the magnitude of material stiffness in the elastic domain was found to be independent of the confining pressure in triaxial tests while governed by chemical bonding of coal particles. Moreover, some researchers have also conducted comparative studies on mechanical properties and energy evolution of soft and hard rock. For example, Huang *et al.* (2021) investigated mechanical behavior and energy evolution characteristics of hard and soft rock by conducting a three-point-bending test with different loading rates. Their test results showed that under the three-point-bending test, the peak load, displacement, total input energy, elastic energy and dissipated energy of both hard and soft rock present linear relationships with the common logarithm of the loading rate.

The loading rate is a significant parameter that determines mechanical strength and deformation of rock (Gao *et al.*, 2020; Xiong and Chen, 2020; Majedi *et al.*, 2021). Cui *et al.* (2021) studied the influence of loading rate on rock tensile strength and split fracture surface morphology, their test results suggested that the rock tensile strength and roughness indices increase with the loading rate. Wang *et al.* (2021) studied the failure mechanism of fractured rock and associated acoustic behavior under different loading rates. They found that with a loading rates increase, the dominant failure modes of fractured sandstones changed from mode-II shear to mode-I tensile fracture. Wisetsaen *et al.* (2015) studied the effects of loading rate and temperature on tensile strength and deformation of rock salt. They found that the salt tensile strengths clearly increased with the applied stress rates for all testing temperatures.

From the above studies, it can be found that the mechanical behavior and energy evolution of single hard and soft rock have been widely reported. However, there are few studies comparing the mechanical behavior and energy evolution characteristics of hard and soft rock under the same conditions. In many soft-hard interbedded rock masses, the hard and soft rock at the same depth not only have the same confining pressure, but also often have the same excavation rate. Therefore, it is of great importance to study the effects of confining pressure and loading rate on the mechanical behavior and energy evolution characteristics of hard and soft rock. The results of the study can provide a guidance for stability, safety and construction efficiency of soft-hard interbedded rock masses.

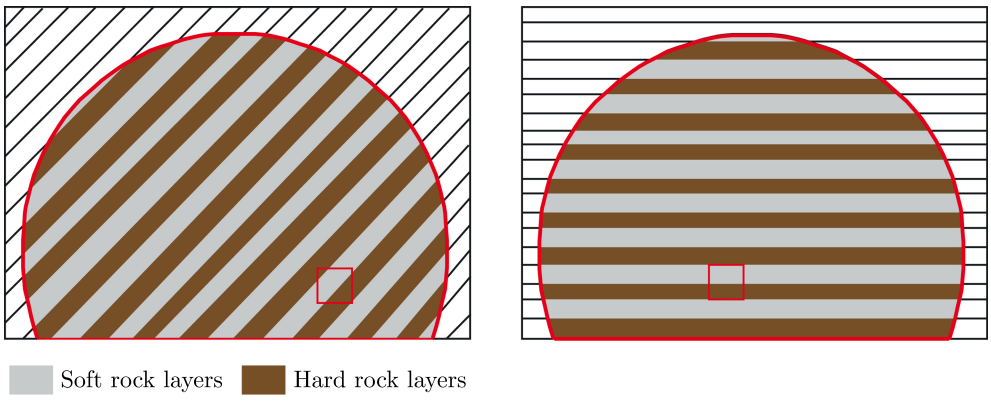

Fig. 1. Tunnel excavation in a soft-hard interbedded rock mass

2. Test methods

2.1. Rock properties and sample preparation

In this study, the tested sandstone and granite were collected from the Three Gorges reservoir area. The main components of sandstone include quartz, feldspar and mica and the main mineral compositions of granite are feldspar, amphibole, quartz and biotite. The average uniaxial compressive strength of sandstone is 112.36 MPa, while the average uniaxial compressive strength of granite is 20.57 MPa. According to the International Society for Rock Mechanics (ISRM) (Lamas, 2017), the tested sandstone and granite can be classified as hard and soft rock, respectively. The physical and mechanical parameters of the sandstone and granite are shown in Table 1.

Table 1. Basic physical and mechanical parameters of sandstone and granite samples

Types	Density [kg/m^3]	Young's modulus [GPa]	Poisson's ratio [–]	UCS [MPa]	UTS [MPa]	Particle size [mm]	Feldspar [%]	Quartz [%]	Amphibole [%]	Mica [%]	Biotite [%]	Other [%]
Sandstone	2325	21.67	0.17	112.36	6.75	0.1∼0.5	41	37	4	12	3	3
Granite	1886	6.64	0.21	20.57	1.87	0.7 ∼ 4	34	29	21	5	9	2

The standard cylindrical samples with a diameter of 50 mm and a height of 100 mm were made by drilling and coring, cutting and section grinding of the complete rock mass. The accuracy of the sample is in accordance with the requirements of the International Society for Rock Mechanics (ISRM) (Fairhurst and Hudson, 1999). Prepared sandstone and granite samples are shown in Fig. 2

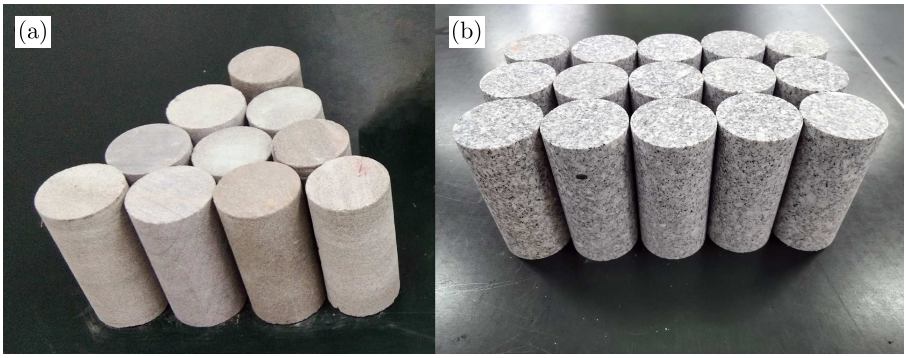

Fig. 2. Prepared rock samples: (a) sandstone, (b) granite

2.2. Test equipment

As shown in Fig. 3a, the TFD-2000 microcomputer servo three-axis rheological testing machine generates the maximum axial force of 2000 kN and the maximum confining pressure of 200 MPa. It includes a data acquisition system, confining pressure control system, axial pressure control system and loading system. The accuracy of both the axial load and confining pressure is 0.001 N. The axial and circumferential deformation of rock samples were measured by axial and circumferential displacement gauges respectively, and the accuracy of the displacement gauges was 0.001 mm. (Fig. 3b).

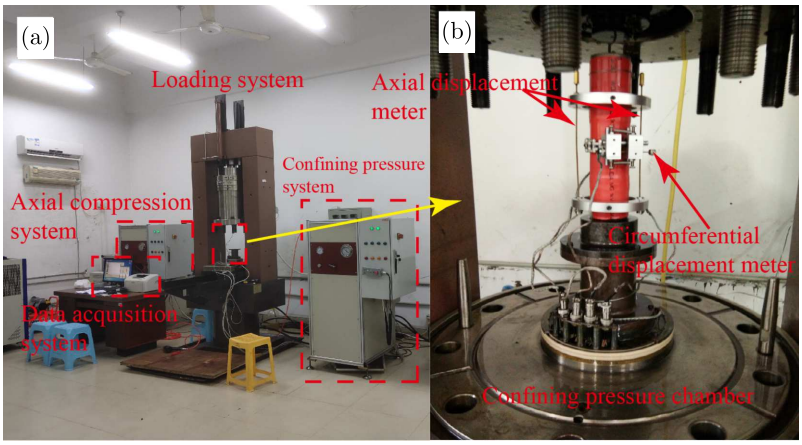

Fig. 3. The triaxial compression testing machine and deformation displacement meter

2.3. Test procedure

Considering that there is some dispersion in the rock mechanics tests, in this study, the rock tests are repeated three times for each condition. The average value is then calculated as the test results for analysis. The detailed test procedure is as follows:

Step 1. The rock sample, wrapped in heat shrink tubing, is fixed to the base of the loading system. Then, the confining pressure chamber is closed and silicone oil is added.

Step 2. Activate the confining pressure control system and apply confining pressure to the specified size at a rate of 0.5 MPa/min. Depending on the sampling depth of the sandstone and granite samples, the confining pressures are designed to 2, 4, 6 and 8 MPa, respectively.

Step 3. When the confining pressure reaches the specified size, the rock sample is at hydrostatic pressure. At this point, the axial stress is applied by displacement loading until failure of the sample. In this study, the three displacement loading rates are 0.01, 0.02 and 0.03 mm/s, respectively.

3. Test results

3.1. Stress-strain curves

The deviatoric stress-strain curves of sandstone and granite under different confining pressure and loading rates are shown in Fig. 4. As can be seen in Fig. 4a,b,c, the deviatoric stress-strain curve of sandstone includes three stages: initial compaction deformation stage, linear-elastic deformation stage and yield deformation stage. The initial compaction deformation stage accounts for a relatively small proportion of the total strain, this indicates that there are fewer original defects (micro-fractures and micro-porosity) within the sandstone. After a short period of compression, the sandstone sample rapidly increases in strength and enters the linear-elastic deformation stage. Then, after a very short yielding deformation stage, the sandstone sample breaks down and the axial stress decreases sharply. Sandstone samples have no residual deformation stage after damage and are typical brittle damage.

The deviatoric stress-strain curves of granite under different confining pressure and loading rates are shown in Fig. 4d,e,f. The deviatoric stress-strain curve of granite includes four stages: initial compaction deformation stage, linear-elastic deformation stage, yield deformation stage and residual deformation stage. The initial compaction deformation stage and the yield deformation stage account for a larger proportion of the total strain. This indicates that there are more original defects (micro-fractures and micro-porosity) within the granite samples and that

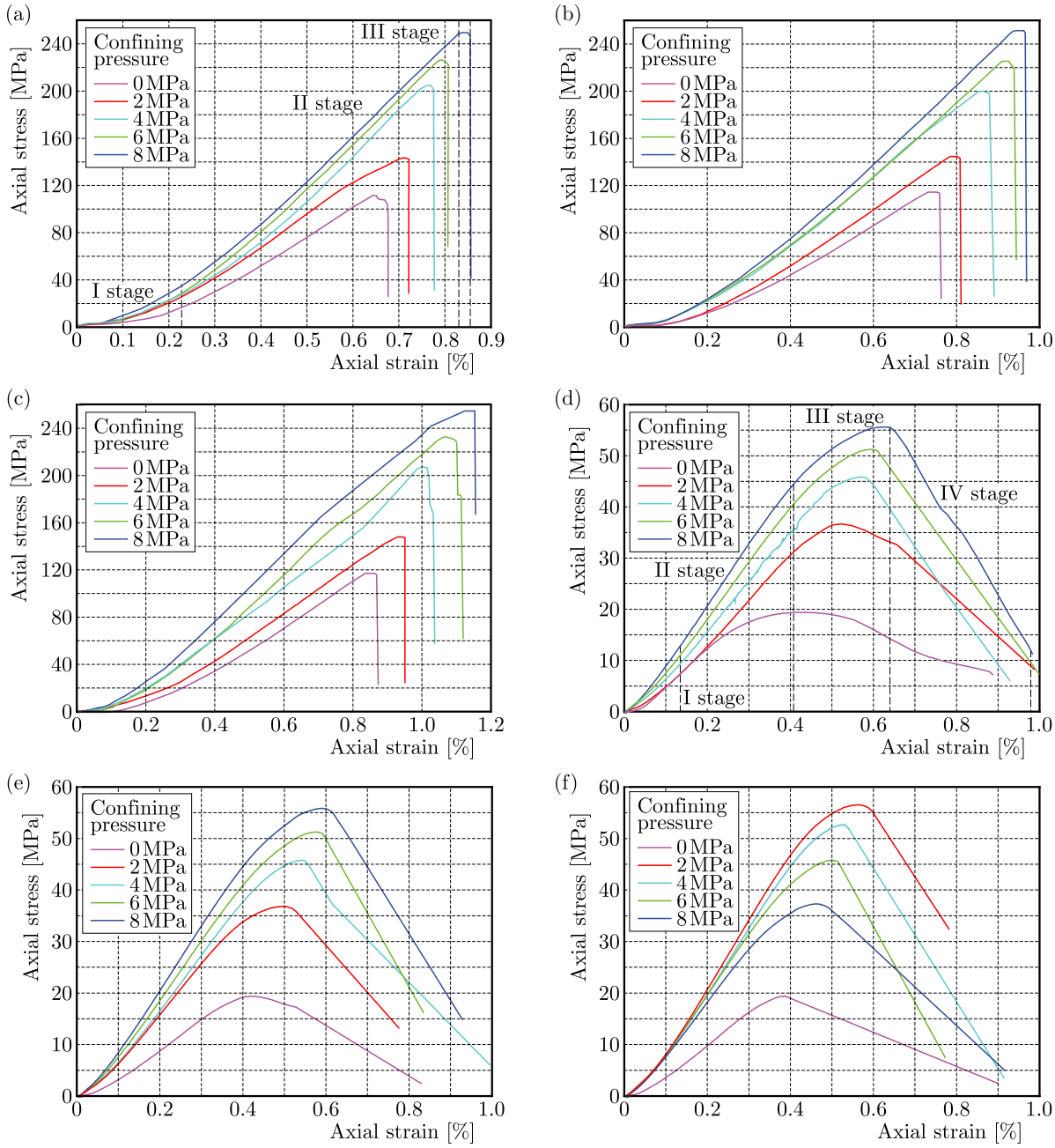

Fig. 4. The deviatoric stress-strain curves of sandstone (a), (b), (c) and granite (d), (e), (f) rock under different confining pressure and loading rates

there is more plastic deformation of the samples before they are damaged. The residual deformation stage means that the load bearing capacity of the granite sample does not disappear immediately after damage, the axial stress decreases slowly with the increasing axial strain.

3.2. Peak strain and peak stress

The relationship between peak axial strain and confining pressure of sandstone and granite is shown in Fig. 5a. The peak axial strain increases with an increase of the confining pressure for both sandstone and granite. When the confining pressure increases from 0 MPa to 2 MPa, and until 8 MPa, the peak axial strain of sandstone average increases by 9.63%, 8.32%, 5.35% and 4.89%, the peak axial strain of granite average increases by 20.35%, 9.06%, 5.21% and 4.59%.

Furthermore, the increase rate of the peak axial strain in sandstone and granite significantly slows with the increasing confining pressure. Figure 5b shows the relationship between the peak axial stress and confining pressure of sandstone and granite. The peak axial stresses in both sandstone and granite increase as the confining pressure increases. When the confining pressure increases from 0 MPa to 2 MPa, and until 8 MPa, the peak axial stress of sandstone average increases by 27.23%, 39.98%, 11.97% and 10.46%, and the peak axial stress of granite average increases by 84.87%, 23.46%, 12.59% and 7.65%. This suggests that although the peak axial stress gradually increases with the increasing confining pressure, the increase rate gradually decreases. Furthermore, when the confining pressure increases from 0 MPa to 2 MPa, the peak axial stress of sandstone average increases by 27.23%, while the peak axial stress of granite average increases by 84.87%. This means that the influence of the confining pressure on the peak axial stress is significantly greater in granite than in sandstone.

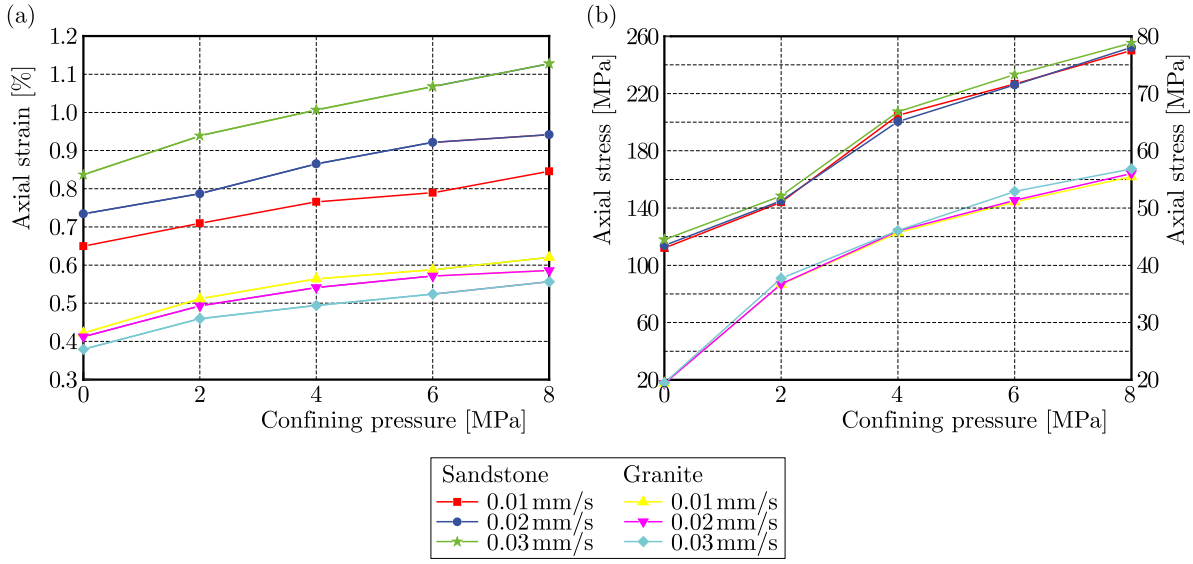

Fig. 5. The relationship among the peak axial strain, peak axial stress and confining pressure of sandstone and granite: (a) peak axial strain, (b) peak axial stress

The relationship between the peak axial strain and loading rate of sandstone and granite is shown in Fig. 6a and Fig. 6b. The peak axial strain of sandstone increases with a growth of the loading rate, while the peak axial strain of granite decreases of the sometime. When the loading rate increases from 0.01 to 0.02 mm/s, and from 0.02 to 0.03 mm/s, the peak axial strain of sandstone average increases by 13.02% and 17.11%, respectively, while the peak axial strain of granite decreases in average by 3.72% and 7.21%, respectively. Figures 6c and 6d show the relationship between the peak axial stress and loading rate of sandstone and granite. When the loading rate increases from 0.01 to 0.02 mm/s, and from 0.02 to 0.03 mm/s, the average peak axial stress of sandstone increases by 0.93% and 2.61%, respectively, and the average peak axial stress of granite increases by 1.01% and 3.19%, respectively. The loading rate has a greater impact on the peak axial stress in granite than in sandstone.

3.3. Ultimate failure pattern

The ultimate failure patterns of sandstone and granite are shown in Fig. 7. The ultimate failure pattern of sandstone is a typical single inclined plane shear failure. When the confining pressure reaches 6 MPa and 8 MPa, the sandstone sample presents a small amount of a wing crack. However, the ultimate failure pattern of granite is more complicated than that of sandstone. When the confining pressure is 0 MPa (uniaxial compression), the ultimate failure

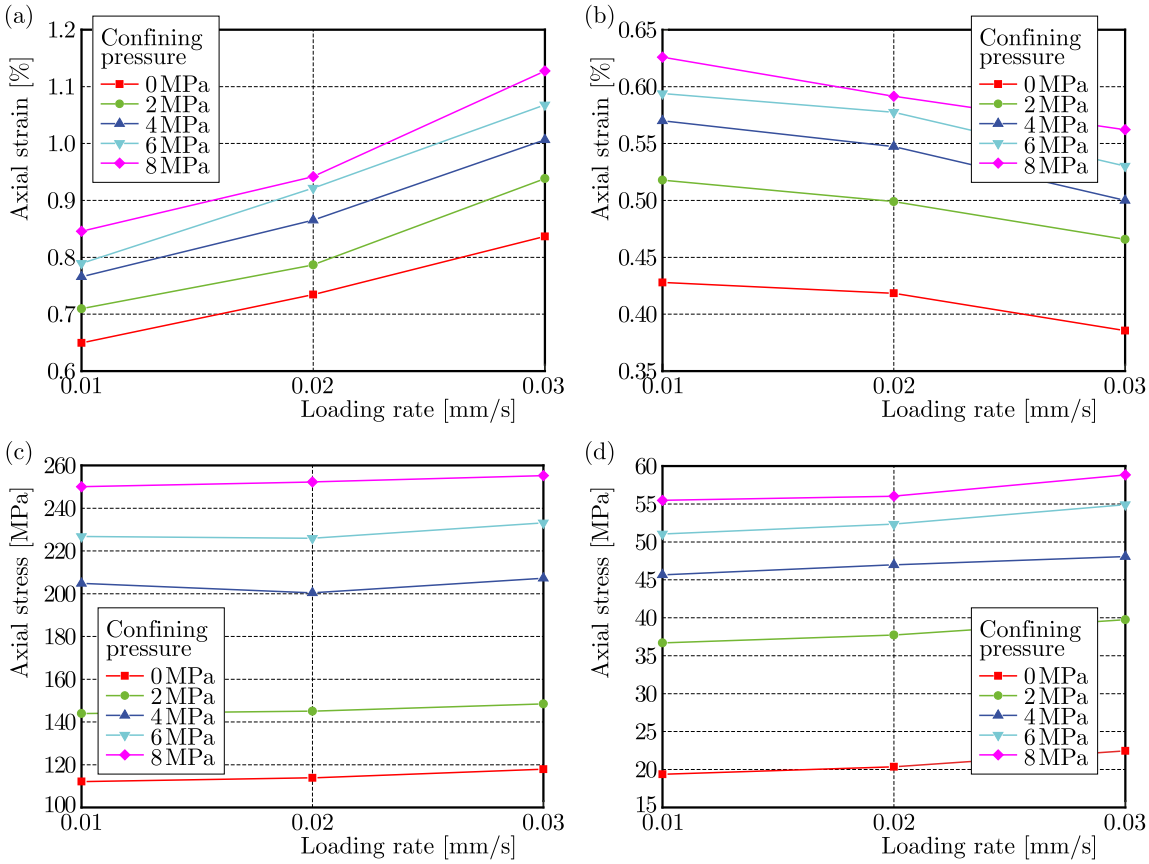

Fig. 6. The relationship among the peak axial strain, peak axial stress and loading rate: (a) peak axial strain of sandstone, (b) peak axial strain of granite, (c) peak axial stress of sandstone, (d) peak axial stress of granite

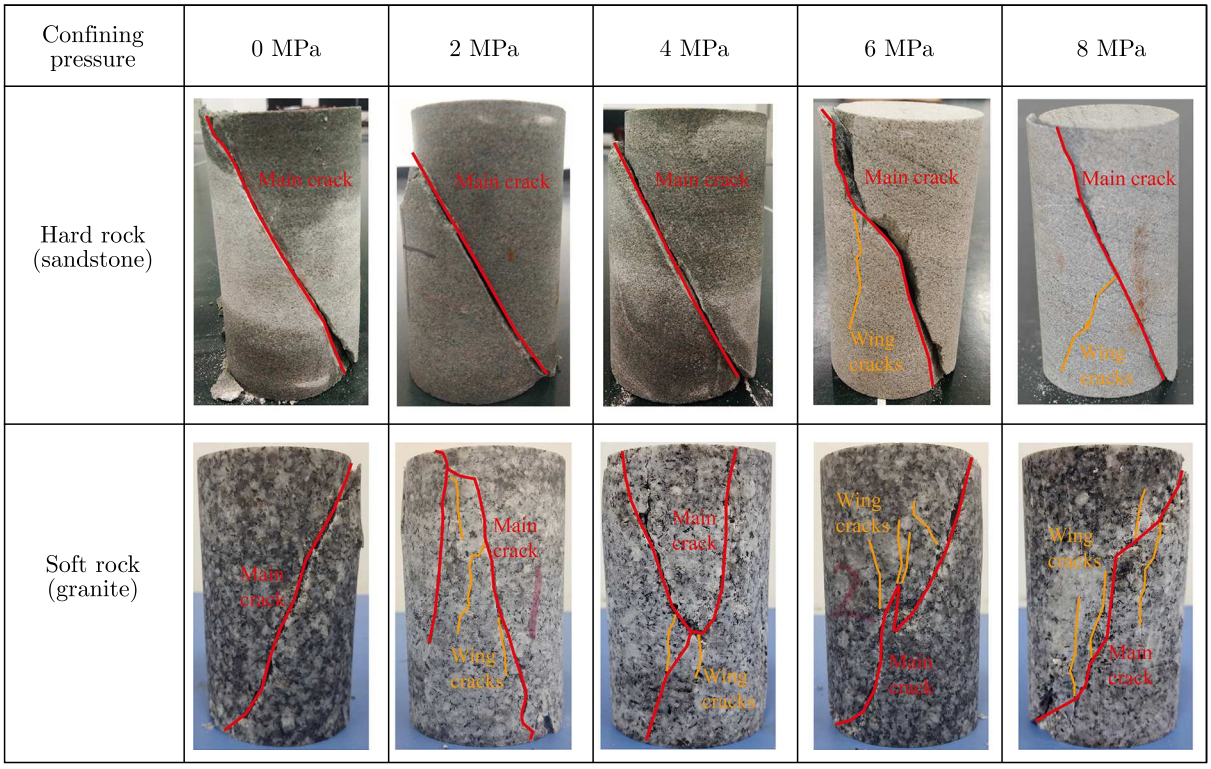

Fig. 7. Ultimate failure pattern of hard and soft rock under different confining pressure

pattern of granite is a typical single inclined plane shear failure and there is no wing crack. As the confining pressure goes up, the ultimate failure pattern of granite samples consists of a single inclined plane shear failure and a vertical split failure. Furthermore, the wing cracks in the granite samples become more and more numerous as the confining pressure increases. The differences in the failure patterns of sandstone and granite also reflect the differences in their deviatoric stress-strain curves. The axial stress in sandstone drops sharply after damage, whereas in granite the axial stress drops slowly after damage. It is worth noting that the loading rate has no significant effect on the macroscopic failure patterns of sandstone and granite and will not be discussed further.

4. Energy evolution

4.1. Calculation of energy

The deformation and damage evolution processes in rock are accompanied by energy conversion, including accumulation, dissipation and release of energy (Huang and Li, 2014; Munoz *et al.*, 2016). Furthermore, lithology, mineral composition and confining pressure of rock have a significant effect on the energy evolution mechanism. In order to analyze the energy evolution of sandstone and granite under different confining pressure and loading rates, the total absorbed energy, elastic energy and dissipated energy are quantitatively determined by the area integral on the stress-strain curves (Fig. 8). Therefore, the total absorbed energy U, elastic energy U_e and dissipated energy U_d can be expressed as

$$U = \int_0^{\varepsilon_2} \sigma_1 \, d\varepsilon \qquad U_e = \int_{\varepsilon_1}^{\varepsilon_2} \sigma_1 \, d\varepsilon \qquad U_d = \int_0^{\varepsilon_2} \sigma_1 \, d\varepsilon - \int_{\varepsilon_1}^{\varepsilon_2} \sigma_1 \, d\varepsilon \tag{4.1}$$

where ε is the axial strain, ε_1 is the permanent deformation after unloading, ε_2 is the peak axial strain, σ_1 is the axial stress.

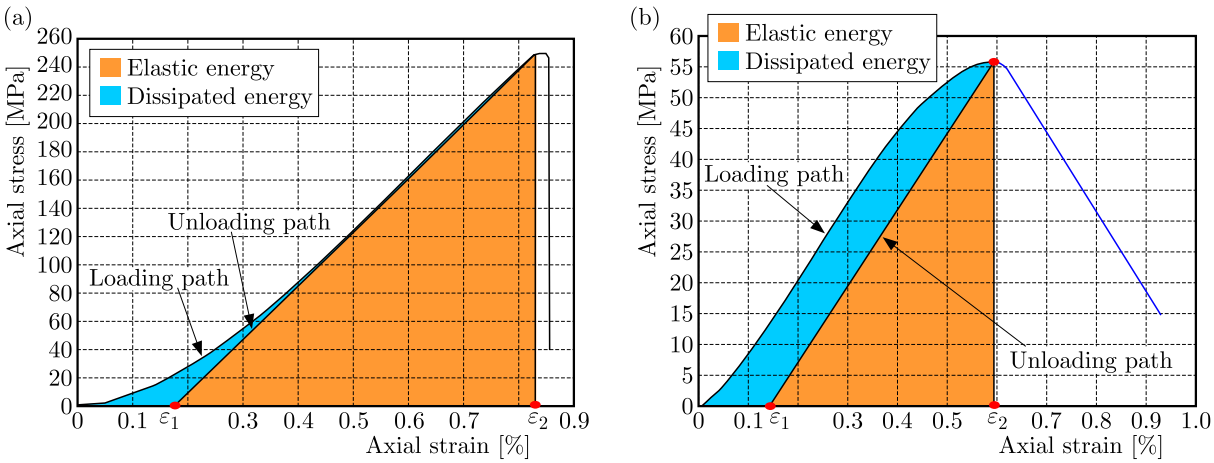

Fig. 8. Calculation of elastic energy and dissipated energy of hard and soft rock

4.2. Effect of confining pressure

The effect of confining pressure on the energy evolution of sandstone is shown in Fig. 9. From Fig. 9a it can be seen that both the total energy and elastic energy increase with a growth of confining pressure, and the dissipated energy first increases and then decreases. When the confining pressure increases from 0 MPa to 2 MPa, and up to 8 MPa, the average total energy

increases by 64.94%, 53.97%, 19.78% and 25.47%, and the average elastic energy increases by 66.21%, 56.39%, 20.09% and 27.13%. Furthermore, when under the same loading rate, the elastic energy is very close to the total energy. This indicates that during compression of the sandstone sample, the vast majority of the energy absorbed from the outside is stored in the sample as elastic deformation with a small amount of energy being dissipated in the plastic deformation of original defects in the sample. The proportion of elastic and dissipated energies to total energy is shown in Fig. 9b. The proportion of elastic energy to total energy increases with the increase of confining pressure, while the proportion of dissipated energy to total energy decreases. The higher the confining pressure, the more the energy absorbed by the sandstone sample is converted into elastic energy and the less the dissipated energy.

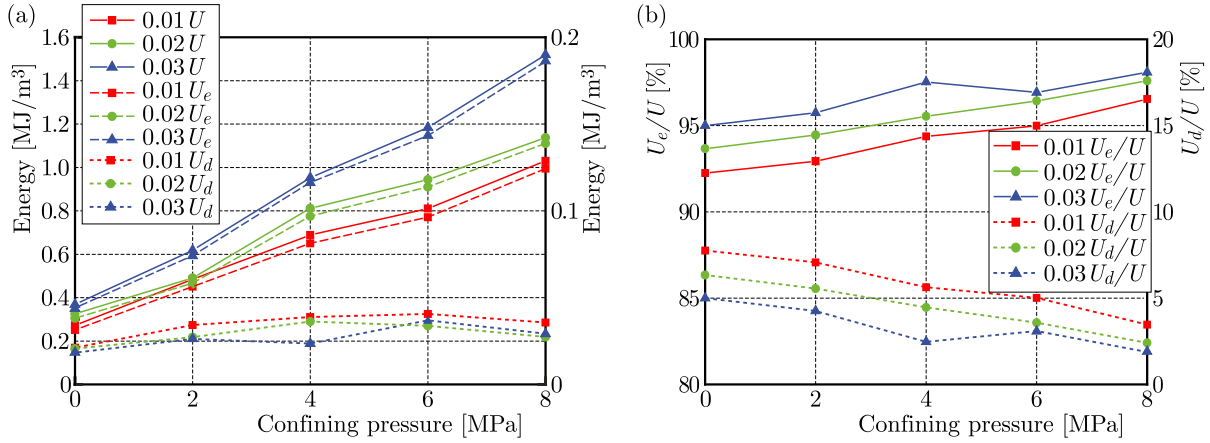

Fig. 9. The effect of confining pressure on energy evolution of sandstone: (a) the total energy, elastic energy and dissipated energy, (b) the proportion of elastic and dissipated energies to total energy

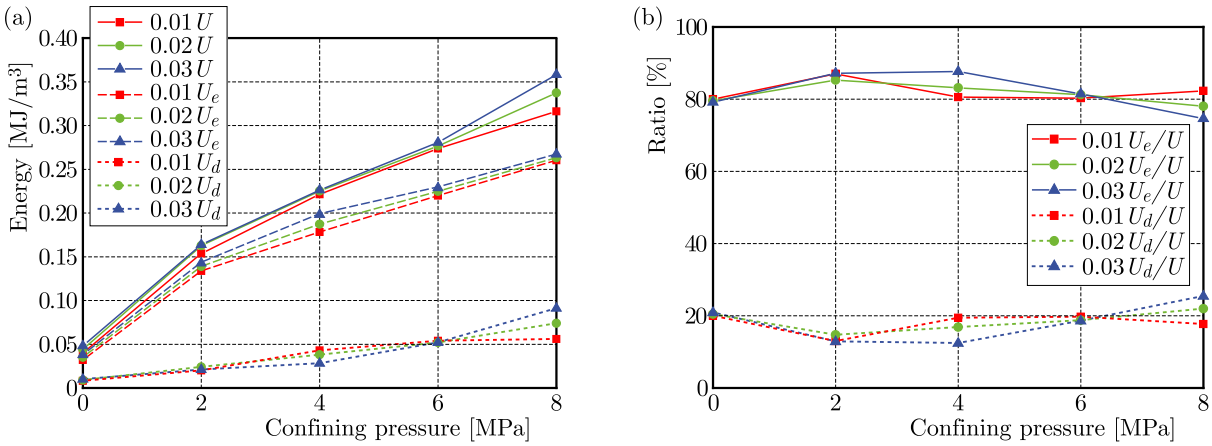

Fig. 10. The effect of confining pressure on energy evolution of granite: (a) the total energy, elastic energy and dissipated energy, (b) the proportion of elastic and dissipated energies to total energy

Figure 10a shows the effect of confining pressure on the energy evolution of granite. The total energy, elastic energy and dissipated energy all increase with the increase of confining pressure. When the confining pressure increases from 0 MPa to 2 MPa, and up to 8 MPa, the average total energy increases by 263.93%, 40.05%, 23.54% and 21.70%, the average elastic energy increases by 295.61%, 35.72%, 19.40% and 17.43%, the average dissipated energy increases by 140.74%, 67.69%, 44.95% and 39.87%. The confining pressure has great influence on the total energy, elastic energy and dissipated energy of granite. It is worth noting that the total energy, elastic energy and dissipation energy all increase as the confining pressure grows, while the increase rate decreases. This indicates that the influence of the confining pressure on deformation of granite

is limited. Furthermore, the difference between the total energy and elastic energy of granite is significantly greater than of sandstone, and the proportion of dissipated energy to total energy of granite is greater than of sandstone. The proportion of dissipated energy to total energy of sandstone is in range 1.91% $\sim$ 7.75% (Fig. 9b), while the proportion of dissipated energy to total energy of granite ranges in 12.82% $\sim$ 25.4% (Fig. 10b).

4.3. Effect of loading rates

The effect of loading rate on the total energy, elastic energy and dissipated energy of sandstone and granite is shown in Fig. 11. It can be found that the total energy and elastic energy

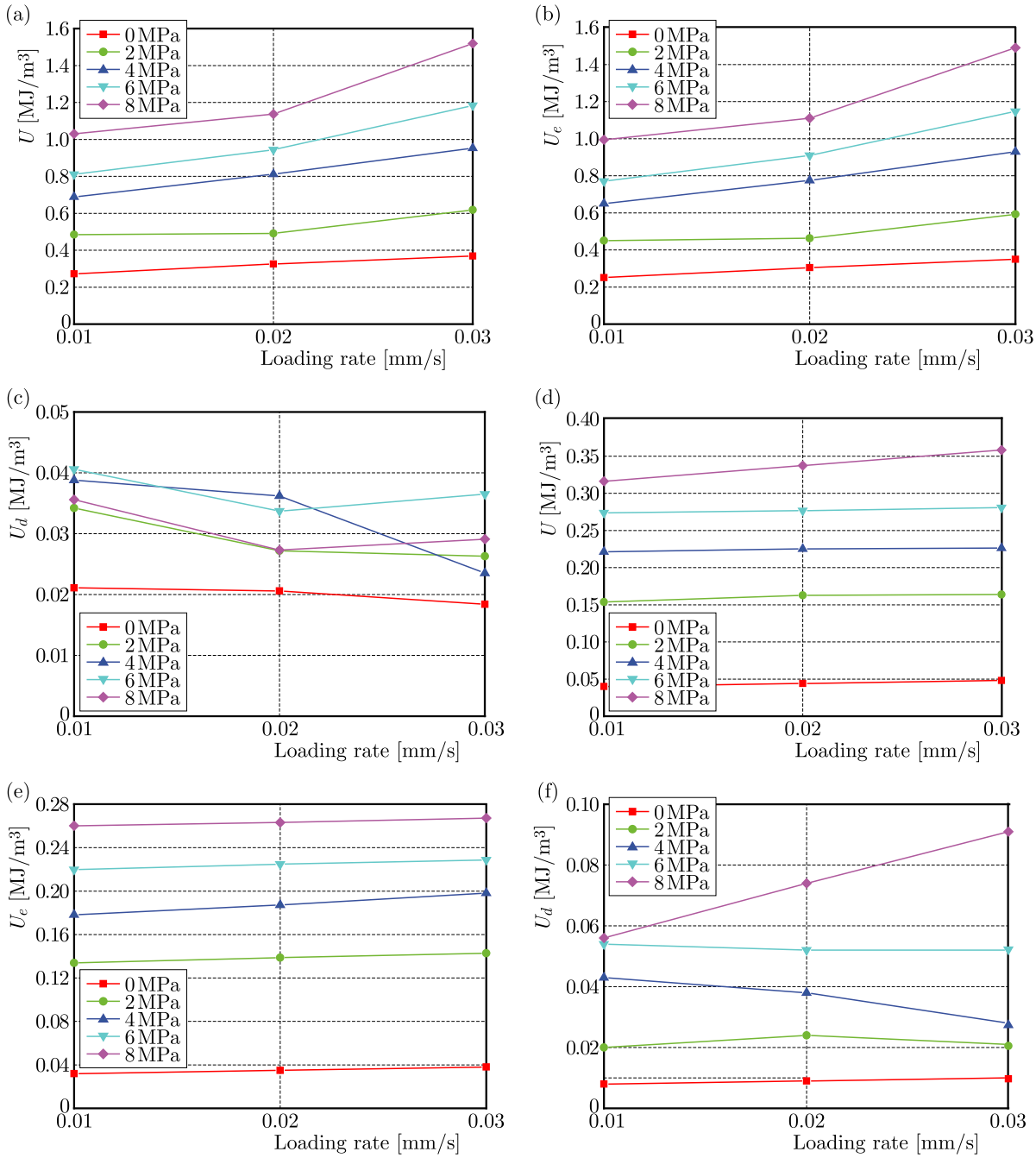

Fig. 11. The effect of loading rate on the: (a) total energy, (b) elastic energy and (c) dissipated energy of sandstone. The effect of loading rate on the: (d) total energy, (e) elastic energy and (f) dissipated energy of granite

of both sandstone and granite increase with growth of the loading rate. The dissipated energy of sandstone decreases with drop of the loading rate, while the dissipated energy of granite increases. Furthermore, it is noteworthy that the loading rate has a very significant effect on the energy evolution of sandstone, yet has a lesser effect on the energy evolution of granite. When the loading rate increases from 0.01 mm/s to 0.02 mm/s, and from 0.02 mm/s to the 0.03 mm/s, for sandstone, the total energy increases in average by 12.84% and 25.18%, the average elastic energy increases by 14.36% and 26.52%, and the average dissipated energy decreases by 14.85% and 7.72%. For granite, the average total energy increases by 4.07% and 2.96%, the average elastic energy increases by 3.03% and 3.06%, and the average dissipated energy increases by 8.83% and 2.53%.

The proportion of elastic and dissipated energies to total energy of sandstone and granite is shown in Fig. 12. When the loading rate increases from 0.01 mm/s to 0.02 mm/s, and from 0.02 mm/s to 0.03 mm/s, the proportion of elastic energy to total energy of sandstone increases by 1.4% and 1.17% (Fig. 12a), while the proportion of elastic energy to total energy of granite first decreases by 0.71% and then increases by 0.69% (Fig. 12b). Meanwhile, the proportion of dissipated energy to total energy of sandstone decreases in average by 22.82% and 25.09% (Fig. 12a), while the proportion of dissipated energy to total energy of granite first increases by 3.25% and then decreases by 3.06% (Fig. 12b). It can be found that the loading rate has a significant effect on the ratio of dissipated energy to the total energy of sandstone. However, the effect of loading rate on the ratios of elastic and dissipated energies to total energy of granite is very small.

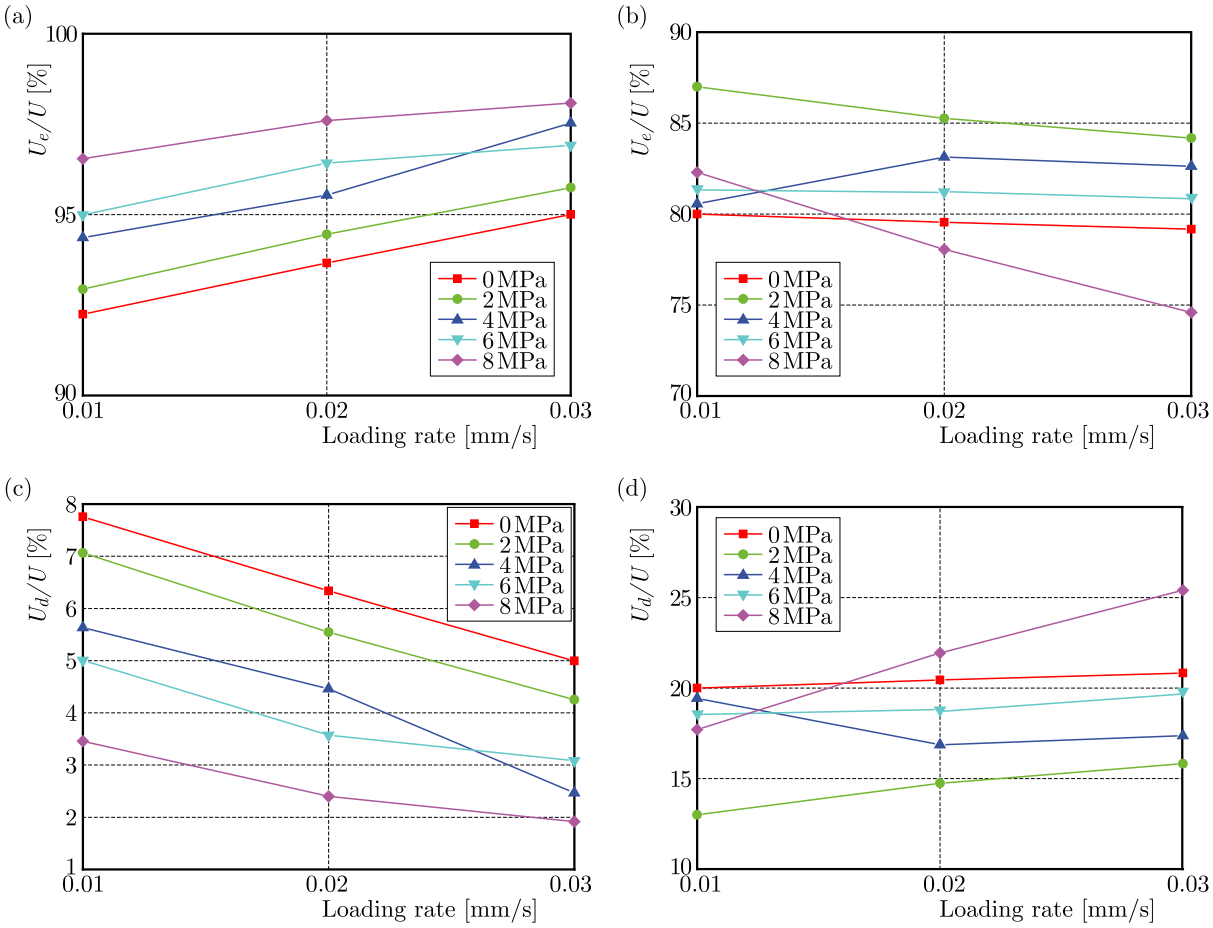

Fig. 12. The proportion of elastic energy to total energy of sandstone (a) and granite (b). The proportion of dissipated energy to total energy of sandstone (c) and granite (d)

5. Conclusion

By carrying out triaxial compression tests of sandstone and granite sample, this study investigated the influence of loading rate and confining pressure on strength, deformation and energy evolution characteristics of hard and soft rock. The main conclusions are summarized as follows:

Table 2. The peak stress and peak strain of sandstone and granite in the triaxial compression test

Rock types	Confining pressure [MPa]	Loading rate [mm/s]					
		0.01		0.02		0.03	
		Stress	Strain	Stress	Strain	Stress	Strain
Sandstone	0	111.98	0.64	112.84	0.73	117.65	0.83
		112.58	0.67	113.47	0.74	116.54	0.79
		113.03	0.66	114.69	0.78	116.98	0.81
	Average	112.53	0.65	113.66	0.75	117.06	0.81
	2	142.98	0.71	145.39	0.79	148.49	0.93
		143.65	0.78	144.97	0.78	148.21	0.94
		142.87	0.69	144.82	0.74	147.65	0.96
	Average	143.17	0.73	145.06	0.77	148.12	0.94
	4	204.78	0.76	200.54	0.86	207.26	1.01
		205.69	0.7	199.87	0.91	206.54	0.98
		204.15	0.74	201.32	0.88	206.17	1.03
	Average	204.87	0.73	200.58	0.88	206.66	1.00
	6	226.78	0.78	225.75	0.92	233.14	1.08
		225.14	0.81	224.98	0.93	232.54	1.07
		227.98	0.73	224.47	0.91	232.37	1.10
	Average	226.63	0.77	225.07	0.92	232.68	1.08
	8	251.07	0.84	252.19	0.94	254.86	1.13
		250.13	0.88	251.57	0.94	255.27	1.12
		249.47	0.81	253.12	0.95	256.12	1.12
	Average	250.22	0.84	252.29	0.94	255.42	1.12
Granite	0	19.37	0.42	19.25	0.41	19.47	0.39
		18.68	0.46	18.68	0.39	19.21	0.38
		18.54	0.43	18.75	0.42	18.96	0.34
	Average	18.86	0.44	18.89	0.41	19.21	0.37
	2	36.64	0.51	36.89	0.49	37.89	0.46
		35.98	0.54	37.14	0.5	38.24	0.41
		35.14	0.54	37.25	0.48	37.59	0.44
	Average	35.92	0.53	37.09	0.49	37.91	0.44
	4	45.61	0.56	45.99	0.54	46.06	0.51
		44.68	0.57	46.21	0.51	47.33	0.49
		43.25	0.56	46.36	0.49	47.21	0.53
	Average	44.51	0.56	46.19	0.51	46.87	0.51
	6	51.06	0.59	51.33	0.57	52.14	0.54
		50.24	0.61	52.02	0.59	52.47	0.53
		49.68	0.58	52.74	0.61	52.91	0.55
	Average	50.33	0.59	52.03	0.59	52.51	0.54
	8	55.47	0.63	56.02	0.59	56.36	0.56
		54.36	0.62	56.89	0.57	55.47	0.58
		54.21	0.64	55.97	0.58	55.18	0.61
	Average	54.68	0.63	56.29	0.58	55.67	0.58

- The peak axial strain and peak axial stress in both sandstone and granite increase with an increase of the confining pressure, and the effect of confining pressure on the peak axial strain and peak axial stress of granite is greater than that of sandstone (Table 2). As the loading rate goes up, the peak axial strain of sandstone increases, while the peak axial strain of granite decreases. The peak axial stresses in both sandstone and granite increase with the increasing loading rates.
- The ultimate failure pattern of sandstone is a typical single inclined plane shear failure, while the ultimate failure pattern of granite consists of a single inclined plane shear failure and a vertical split failure. With the increase of confining pressure, wing cracks appear in both sandstone and granite. The loading rate has no significant effect on the macroscopic failure pattern of sandstone and granite.
- The total energy, elastic energy and dissipated energy of sandstone and granite increase with the increase of confining pressure. As the confining pressure increases, the proportion of the sandstone elastic energy to the total energy increases and the proportion of dissipated energy decreases. However, the proportion of granite elastic energy to the total energy decreases and the proportion of dissipated energy increases. The effect of confining pressure on the total energy, elastic energy and dissipation energy of granite is greater than that of sandstone.
- The total energy and elastic energy of both sandstone and granite increase with growth of the loading rate. The dissipated energy of sandstone decreases with drop of the loading rate, while the dissipated energy of granite increases. The loading rate has a small effect on the proportion of elastic and dissipated energies to the total energy of sandstone and granite.

It is worth noting that the identifying of the failure of the sample surface is important for subsequent modelling of both soft and hard rock samples. Therefore, it will be considered in a future work.

Acknowledgments

This work is supported by the National Natural Science Foundation of China (Nos. 41807279 and 41972297) and the Natural Science Foundation of Hebei Province, China (No. E2019202336).

References

1. Alam A.K.M.B., Fujii Y., Fukuda D., Kodama J., Kaneko K., 2015, Fractured rock permeability as a function of temperature and confining pressure, *Pure and Applied Geophysics*, **172**, 2871-2889
2. Asem P., 2019, Base resistance of drilled shafts in soft rock using in situ load tests: A limit state approach, *Soils and Foundations*, **59**, 6, 1639-1658
3. Chen Z.Q., He C., Hu X.Y., Ma C.C., 2021, Effect of stress paths on failure mechanism and progressive damage of hard-brittle rock, *Journal of Mountain Science*, **18**, 2486-2502
4. Cui Z, Qian S, Zhang G.M., Maochu Z., 2021, An experimental investigation of the influence of loading rate on rock tensile strength and split fracture surface morphology, *Rock Mechanics and Rock Engineering*, **54**, 1969-1983
5. Fairhurst C.E., Hudson J.A., 1999, Draft ISRM suggested method for the complete stress-strain curve for the intact rock in uniaxial compression, *International Journal of Rock Mechanics and Mining Sciences*, **36**, 3, 279-289
6. Fereidooni D., Khanlari G., Heidari M., Sepahigero A.A., Kolahi-Azar A.P., 2016, Assessment of inherent anisotropy and confining pressure influences on mechanical behavior of

anisotropic foliated rocks under triaxial compression, *Rock Mechanics and Rock Engineering*, **49**, 2155-2163

7. Gao M.Z., Zhang J.G., Li S.W., Wang M., Wang Y.W., Cui P.F., 2020, Calculating changes in fractal dimension of surface cracks to quantify how the dynamic loading rate affects rock failure in deep mining, *Journal of Central South University*, **27**, 3013-3024
8. Hu B., Yang S.Q., Xu P., Cheng J.L., 2019, Cyclic loading-unloading creep behavior of composite layered specimens, *Acta Geophysica*, **67**, 449-464
9. Huang D., Li Y.R., 2014, Conversion of strain energy in triaxial unloading tests on marble, *International Journal of Rock Mechanics and Mining Sciences*, **66**, 160-168
10. Huang D., Liu Y., Yang Y.Y., Li Z., Meng Q., 2021, Experimental study on three-point-bending characteristics of hard and soft rock-like materials under different loading rates, *Arabian Journal of Geosciences*, **14**, 1951
11. Karami M., Tolooiyan A., 2020, Investigating the elastoplasticity of an Australian soft rock based on laboratory test results, *Engineering Geology*, **276**, 105762
12. Kavvadas M., Roumpos C., Schilizzi P., 2020, Stability of deep excavation slopes in continuous surface lignite mining systems, *Geotechnical and Geological Engineering*, **38**, 791-812
13. Lamas L., 2017, International Society for Rock Mechanics – ISRM, [In:] *Encyclopedia of Engineering Geology*, P. Bobrowsky, B. Marker (Edit.), Encyclopedia of Earth Sciences Series, Springer, Cham
14. Majedi M.R., Afrazi M., Fakhimi A., 2021, A micromechanical model for simulation of rock failure under high strain rate loading, *International Journal of Civil Engineering*, **19**, 501-515
15. Munoz H., Taheri A., Chanda E.K., 2016, Rock drilling performance evaluation by an energy dissipation based rock brittleness index, *Rock Mechanics and Rock Engineering*, **49**, 3343-3355
16. Pinazzi P.C., Spearing A.J.S., Jessu K.V., Singh P., Hawker R., 2021, Combined load failure criterion for rock bolts in hard rock mines, *Mining Metallurgy and Exploration*, **38**, 427-432
17. Sengani F., 2020, Characterisation of rock fracturing ahead of the preconditioned mining faces in a hard rock mining, *Arabian Journal of Geosciences*, **13**, 670
18. Wang X.R., Wang E.Y., Liu X.F., Zhou X., 2021, Failure mechanism of fractured rock and associated acoustic behaviors under different loading rates, *Engineering Fracture Mechanics*, **247**, 107674
19. Wisetsaen S., Walsri C., Fuenkajorn K., 2015, Effects of loading rate and temperature on tensile strength and deformation of rock salt, *International Journal of Rock Mechanics and Mining Sciences*, **73**, 10-14
20. Xiong L.X., Chen H.J., 2020, Effects of high temperatures and loading rates on the splitting tensile strength of jointed rock mass, *Geotechnical and Geological Engineering*, **38**, 1885-1898

Manuscript received May 26, 2022; accepted for print June 12, 2022